ISSN 0974-3618 (Print)
0974-360X (Online)

www.rjptonline.org

RESEARCH ARTICLE

Structure-based Pharmacophore Modelling for identifying VEGFR2 Inhibitor

Muhammad Arba*, Jasriati Jasriati
Faculty of Pharmacy, Universitas Halu Oleo, Kendari, Indonesia - 93231
*Corresponding Author E-mail: **muh.arba@uho.ac.id**

ABSTRACT:
The vascular endothelial growth factor (VEGF) plays a crucial role in a wide range of cellular functions particularly in the angiogenesis process. Overexpression of vascular endothelial growth factor receptor (VEGFR) leads to several disease including cancer. Inhibition of the VEGFR constitutes the major strategies for combating cancer growth. The current investigation was aimed at identifying potential inhibitor of VEGFR2 by using structure-based pharmacophore modelling using LigandScout 4.3. Advanced software. The pharmacophore hypothesis consisted of 4 hydrophobic, one hydrogen bond donor, and two hydrogen bond acceptors, which was built using the structure of cognate ligand of VEGFR2 (608). Further, the pharmacophore model was used to screen hit molecule against ZINC database using Pharmit. Further, 102 virtual hits were retrieved, which were submitted to molecular docking simulation by employing iDock software. Molecular dynamics simulation of 50 ns for each three best hits complexed with VEGFR2 indicated that each ligand underwent minor conformational changes as indicated by the values of Root Mean Square Deviation (RMSD) and Root Mean Square Fluctuation (RMSF). Prediction of affinities employing Molecular Mechanics Poisson-Boltzmann Surface Area (MM-PBSA) method identified one hit molecule (i.e. Lig5/ZINC33025328) with significant affinity lower than that of cognate ligand, which indicated its potential as a novel VEGFR2 inhibitor.

KEYWORDS: VEGFR2, molecular dynamics simulation, virtual screening; pharmacophore model, Ligand Scout

INTRODUCTION:
Vascular endothelial growth factor receptor (VEGFR) is one of the protein kinases, which participates in the formation of new blood vessel or neovascularization including those from angioblasts (vasculogenesis) and those from pre-existing vasculature (angiogenesis) (1). Angiogenesis is known to play a key role in the progression of cancer as tumor growth requires much higher amount of new capillaries formation. Therefore, cancer is one of the diseases which can potentially be treated by curbing of VEGF signaling (2). The VEGF receptors consist of VEGFR-1 (Flt-1, feline McDonough sarcoma virus-like tyrosyl kinase-1), VEGFR-2 (Flk-1/kinase domain receptor, KDR, fetal liver kinase-1/Kinase insert Domain-Containing Receptor) and VEGFR-3 (Flt-4) (3-4).

Received on 27.09.2019 Modified on 25.10.2019
Accepted on 23.11.2019
Research J. Pharm. and Tech. 2020; 13(7): 3129-3134.
DOI: 10.5958/0974-360X.2020.00553.3

VEGFR structures contain an extracellular segment, a transmembran segment, a juxtamembran segment, an intracellular protein-tyrosine kinase domain, and a carboxyterminal domain (5). The VEGFR1 has VEGF-A, VEGF-B, and P1GF as endogenous ligands, while VEGFR2 and VEGFR3 share the same VEGF-C and VEGF-D as pro-angiogenic factors in addition to VEGF-A, VEGF-E, and VEGF-F, which belong to VEGFR2 (2,6). The VEGFRs can be found in vascular endothelial cells (VEGFR1 and VEGFR2) and in lymphatic endothelial cells (VEGFR3) (7).

The catalytic domain of those VGFRs contains about 330 amino acids as a result of additional inserts of about 70 residues in addition to 250-300 amino acid of traditional catalytic domains (8). They have the smaller N-terminal lobe containing five β-strands (β1-β5) and a regulatory αC-helix, and the larger C-terminal lobe containing seven helices (αD- αI and αEF) and four short β-strands (β6-β9) (9). Between the two lobes, there is a cleft, where ATP nucleotide substrate interacts, which consisted of the two lobes residues.

Compared to VEGFR1 and VEGFR3, VEGFR2 is the most prominent activator of migration, proliferation, survival, and enhanced vascular permeability of endothelial cell (1). It displays predominant protein kinase activity originating from autophosphorylation on six tyrosine residues of the receptor within the activation loop (1,10,11) when interacting with its endogenous ligands (12). The VEGF/VEGFR2 signalling pathway is often overexpressed in the growth and metastasis of human cancer. Therefore, VEGFR-2 is thought to be the key target for discovering small molecule inhibitors against tumor-associated angiogenesis.

Many small molecules inhibitors of VEGFR-2 protein kinases have been developed such as imatinib, sorafenib, and sunitinib. Imatinib has been known for its use to treat gastrointestinal stromal tumors and chronic myelogenous leukemia (CML) since 2001 (13). Sorafenib was approved by Food and Drug Administration (FDA) in 2005 for the treatment of metastatic renal cell carcinoma (1). Sunitinib was taken for clinical use in 2006 for the treatment of metastatic renal cell carcinoma and gastrointestinal stromal tumors (14). However, drug resistance and low selectivity remain a challenge and new small molecule inhibitors of VEGFR2 are still urgently needed.

The present work is aimed to identify the potential of VEGFR2 inhibitors by using pharmacophore-based virtual screening method. The pharmacophore-based virtual screening, which use a crystal structure of protein-ligand complex, has been widely recognized as an integral part of drug discovery stages (15-20). The method was combined with docking and molecular dynamics (MD) simulation to reveal the ligand binding modes and their conformational changes during a certain period of time (12-24). Finally, binding affinity evaluation of ligand was performed by using Molecular Mechanics Poisson Boltzmann Surface Area (MM-PBSA) method.

COMPUTATIONAL METHODS:

Pharmacophore modeling:

The pharmacophore model was developed using LigandScout 4.3 software (25). The software builds models of pharmacophore using 3D structure of protein-ligand complex. In this case, VEGFR2 kinase domain structure in complex with an inhibitor (a nicotinamide, 608) was downloaded from RCSB Protein Data Bank with the PDB code 2P2I (26). Validation of the pharmacophore hypothesis was performed by using actives and decoys compounds, which were taken from the Directory of Useful Decoys-Enhanced (DUD-E) (27). Further, the built pharmacophore model was employed to identify hits in the ZINC15, a free database of compounds (28) using Pharmit web server (http://pharmit.csb.pitt.edu/) (29).

Molecular docking, molecular dynamics studies, and prediction of the binding free energy:

Molecular docking for 102 compounds on VEGFR2 was performed using iDock software (30-32). The iDock essentially uses AutoDock Vina scoring function but with additional features, enabling large number of compounds to be screened. Therefore, it was efficient enough to predict ligand binding modes and affinity at affordable computational cost. Docking protocol was validated by redocking the native inhibitor of VEGFR2 (608). The binding site of VEGFR2 was set following the coordinates of 608, while the grid box was applied with a size of 22.5 × 22.5 × 22.5 Å in XYZ dimensions.

Further analysis was performed based on the binding mode and affinity of each compound and three top compounds having the highest binding affinities were subjected for further molecular dynamics (MD) simulation.

Four molecular dynamics (MD) simulations were conducted using three best hits and one native ligand docked complexes. MD studies were performed using the PMEMD engine of Amber 16 package (33,34). Protein and ligand were parameterized using the force fields of ff14SB (35) and GAFF (36) as well as AM1-BCC (37). All system preparation for MD simulation and binding free energy prediction were explained in our previous works (38,39).

RESULTS AND DISCUSSION:

Virtual screening methods has been widely known particularly in the early drug discovery processes. The method involves the exploitation of computer-aided techniques to identify potential inhibitors for specific therapeutic targets (39). Virtual screening can be divided into structural-based approach and ligand-based screening, including pharmacophore modelling. The pharmacophore modelling was then grouped as structural-based and ligand-based approaches. The structure-based pharmacophore modelling uses protein-ligand complex, while the ligand-based approach only utilizes ligand structure. The present study employs structure-based pharmacophore modelling to search for hits of VEGFR2. Structure of VEGFR2 and a nicotinamide (608) was used to build pharmacophore model consisting of four hydrophobic, two H bond acceptor, and one H Bond donor. Figure 1 shows the pharmacophore model.

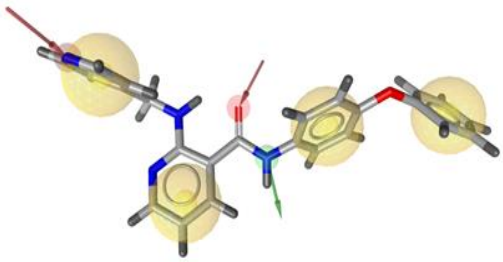

Figure 1: 3D pharmacophore features extracted from LigandScout 4.3, which consisted of the hydrophobic (yellow), hydrogen bond donor (green), and hydrogen bond acceptors (red sphere).

The validation of pharmacophore model was conducted by screening the model against internal database, which consisted of 619 actives and 25247 decoys. The result showed that the value of Receiver Operating Characteristic-Area Under Curve (ROC-AUC) is 0.51, while GH-score is 0.75. Therefore, the developed pharmacophore hypothesis was valid. Fig. 2 displays the ROC curve.

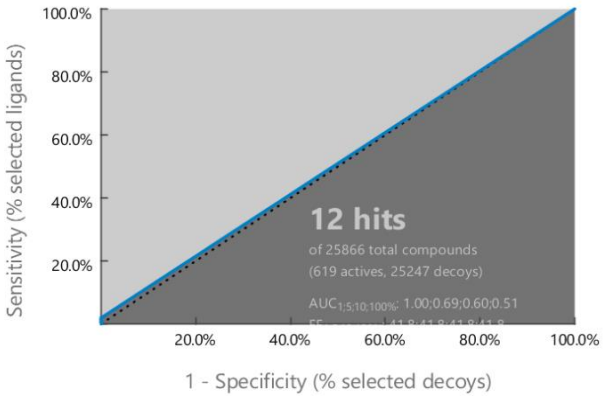

Figure 2: The receiver operator characteristic curve with area under curve (AUC) 100%=0.51.

Further, the pharmacophore model was used for screening hits in ZINC database using Pharmit (http://pharmit.csb.pitt.edu/), with "Max Hits per Conf"=1, yielded 102 hits. The molecular docking of all 102 hit compounds on VEGFR2 gave poses and affinities in the range of −4.11 and −13.02 kcal/mol, while redocking of 608 yielded affinity of −12.45 kcal/mol. Two hit compounds displayed affinities lower than that of 608, i.e. Lig9/ZINC33258090 (E=−13.02 kcal/mol) and Lig5/ZINC33025328 (E= −12.96 kcal/mol).

Redocking of 608 produced a pose which is essentially identical with the X-ray conformation with root mean square deviation (RMSD) of 1.04 Å, indicating that the docking protocol was valid (40). The docked conformation reproduced all three experimental hydrogen bonds (hbonds) with Glu885, Cys919, and Asp1046. Figure 3 presents the 608 poses of both x-ray and docked structures.

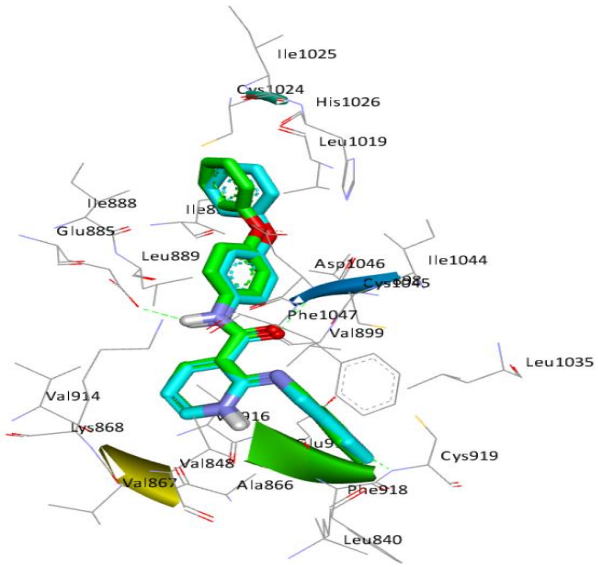

Figure 3: Superimposed structures of docked (green) and x-ray (blue) of 608. The green-colored dashed lines indicate the hydrogen bond interactions.

Furthermore, three best docked hits were selected, which is Lig9/ZINC33258090, Lig5/ZINC33025328, and Lig90/ZINC09441733. Figure 4 presents the chemical structures of three best hit compounds resulted from molecular docking.

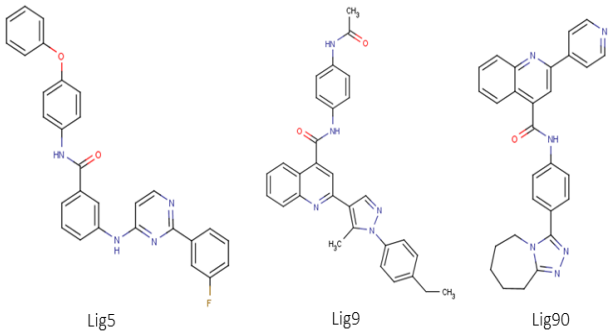

Figure 4: The chemical structures of best 3 hit compounds.

The Lig9/ZINC33258090 interacted with crucial amino acid residues of VEGFR2. The amino group of Lig9/ZINC33258090 contributed as hbond donor when interacting with Cys919 residue. The Cys919 residue was also observed to contribute in hbond formation with pyrimidine group of Lig5/ZINC33025328. Meanwhile, the same residue interacted through van der Waals interaction with Lig90/ZINC09441733. As previously described, Cys919 residue constituted crucial amino acid residues of active site, which formed hbond interaction with 608. Figure 5 shows the interaction of Lig5, Lig9, Lig90 in the VEGFR2.

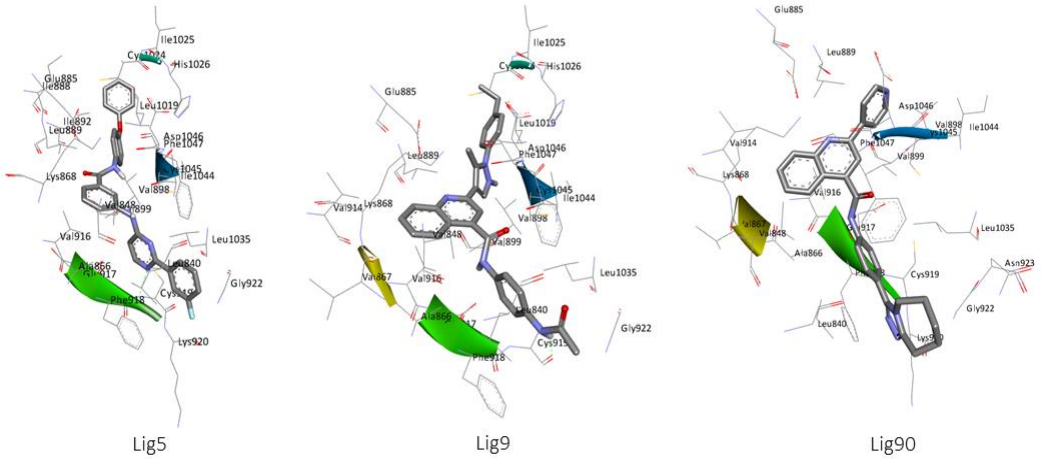

Figure 5: The interaction of Lig5, Lig9, Lig90 in the VEGFR2 with hydrogen bonds (green dashed lines).

Molecular dynamics simulations:

MD simulation was performed for each VEGFR2-ligand complex to assess the conformational changes for 50 ns. The values of root mean square deviation (RMSD) were calculated to verify the stability of complex. Figure 6a and 6b display RMSD values of heavy atoms (Cα, C, N, O) of the protein and ligand, respectively, showing that all ligands maintained the stability throughout simulation. The Lig5 and Lig90 reached equilibrium quickly with stable RMSD around 2 Å. Lig9 slightly fluctuated at around 30 ns. However, it became stable for the rest simulation. Interestingly, all hits showed more stable movement than cognate ligand (608).

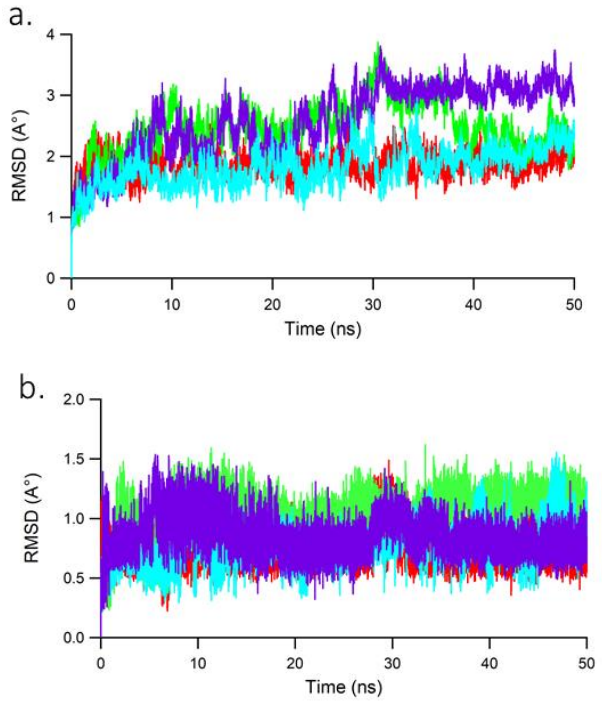

Figure 6: RMSD values of heavy atoms of (a) the protein and (b) ligand, respectively, for (a) LIG5 (red), Lig9 (green), Lig90 (blue), and 608 (purple).

Figure 7 depicts root mean square fluctuation (RMSF) plot for 50 ns MD run. It shows that ligand binding induced similar pattern of amino acid residues fluctuation and minor change during MD simulation. The highest RMSF value was at the His289 (His1178) corresponding to the carboxy terminal of the protein. Peak at around Ala118 (Ala991) was loop region, which was principally more fluctuated than other regions of protein.

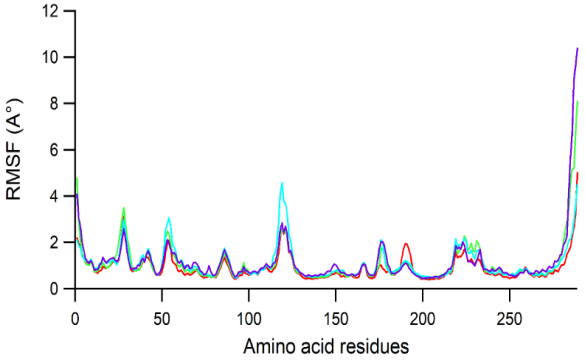

Figure 7: RMSF plot for 50-ns MD simulation: (a) LIG5 (red), Lig9 (green), Lig90 (blue); (b) 608 (purple).

Monitoring of the hbonds during dynamics runs showed that the hbonds interactions with Cys919 attained occupancies of 38.60% and 22.25% in the Lig9/ZINC33258090 binding, while those in the Lig90/ZINC09441733 attained 11.98% and 5.13% occupancies. The lower occupancy was detected as 3.24% in the binding of Lig5/ZINC33025328. Interestingly, Lig5/ZINC33025328 showed high hbond occupancies with Glu885 and Asp1046 residues each with 57.93% and 20.09%, respectively. In brief, the moderated occupancies were recorded in the binding of Lig5/ZINC33025328 and Lig9/ZINC33258090, while those in the binding of Lig90/ZINC09441733 showed lower occupancies. Table 1 shows the hbond occupancies during 50-ns simulation.

Table 1: The hydrogen bond occupancies during 50-ns MD simulation.

Ligand	Acceptor	Donor	Occupancy (%)	Distance (Å)	Angle
Lig9/ZINC33258090	Lig@O1	Cys_919@H: Cys_919@N	38.60	2.84	158.77
	Cys_919@O	Lig@H24: Lig@N4	22.25	2.86	157.67
Lig5/ZINC33025328	Glu_885@OE1	Lig@H5: Lig@N	57.93	2.84	156.27
	Lig@O	Asp_1046@H: Asp_1046@N	20.09	2.89	158.37
	Lig@N3	Cys_919@H: Cys_919@N	3.24	2.95	159.02
Lig90/ZINC09441733	Lig@N3	Cys_919@H: Cys_919@N	11.98	2.94	156.93
	Lig@N4	Cys_919@H: Cys_919@N	5.13	2.95	156.64

Table 2: The binding free energy terms (kcal/mol).

Ligand	ΔE_{ELE}	ΔE_{VDW}	ΔE_{PBCAL}	ΔE_{PBSUR}	ΔE_{PBTOT}
608	−28.82±3.58	−58.42±3.13	52.25±2.84	−4.99±0.08	−39.98±3.34
Lig5	−25.23±3.28	−67.32±2.73	50.84±2.82	−5.65±0.09	−47.37±3.74
Lig9	−14.68±4.54	−67.98±3.40	52.79±7.64	−6.12±0.11	−35.99±4.32
Lig90	−11.90±4.54	−63.04±3.38	46.29±5.15	−5.40±0.14	−34.05±4.09

Free binding energy calculations:

The binding free energy was calculated using MM-PBSA method to reveal each individual energy contribution to the complex stability. The electrostatic (ΔE_{ELE}), van der Waals (ΔE_{VDW}), polar solvation energy (ΔE_{PBCAL}), and non-polar solvation energy (ΔE_{PBSUR}), for each c omplex are presented in Table 2. The total binding energy (ΔE_{PBTOT}) for each complex was negative (from −34 to −47 kcal/mol), indicating the attraction interaction. Interestingly, Lig5 achieved the highest affinity among other hits. The electrostatic energy, van der Waals energy, and non-polar solvation energy were favourable for ligand binding, while polar solvation energy opposed ligand binding.

CONCLUSION:

Structure-based pharmacophore modelling was conducted based on protein-ligand complex structure. The pharmacophore hypothesis was used to screen hit in ZINC database. It obtained 102 hits and molecular docking was conducted to probe the binding mode of each hit. Three best docked hits were subjected to molecular dynamics simulation, showing the stable changes during 50 ns. The MM-PBSA method identified one potential hit (Lig5/ZINC33025328) as VEGFR2 inhibitor. The van der Waals and electrostatic interactions were favorable for ligand binding. The present study suggests one potential ligand for further experiment validation.

ACKNOWLEDGEMENT:

The authors are grateful to the Ministry of Research, Technology, and Higher Education, Republic of Indonesia for funding this work.

CONFLICT OF INTEREST:

The authors declare no conflict of interest.

REFERENCES:

1. Roskoski R. VEGF receptor protein–tyrosine kinases: Structure and regulation. Biochemical and Biophysical Research Communications. 2008: 375; 287–291.
2. Roskoski R. Vascular endothelial growth factor (VEGF) signaling in tumor progression. Critical Reviews in Oncology/Hematology. 2007: 62; 179–213.
3. Terman BI, Carrion ME, Kovacs E, Rasmussen BA, Eddy RL and Shows TB. Identification of a new endothelial cell growth factor receptor tyrosine kinase. Oncogene. 1991: 6; 1677–1683.
4. Terman BI, Dougher-Vermazen M, Carrion ME, Dimitrov D, Armellino DC, Gospodarowicz D and Bohlen P. Identification of the KDR tyrosine kinase as a receptor for vascular endothelial cell growth factor. Biochemical and Biophysical Research Communications. 1992: 187; 1579–1586.
5. Roskoski R. Vascular endothelial growth factor (VEGF) and VEGF receptor inhibitors in the treatment of renal cell carcinomas. Pharmacological Research. 2017: 120; 116–132.
6. Simons M, Gordon E and Claesson-Welsh L. Mechanisms and regulation of endothelial VEGF receptor signalling. Nature Reviews Molecular Cell Biology. 2016: 17; 611-625.
7. Hoeben A, Landuyt B, Highley MS, Wildiers H, Oosterom ATV and De Bruijn EA. Vascular Endothelial Growth Factor and Angiogenesis. Pharmacological Reviews. 2004: 56; 549-580.
8. Locascio LE, Donoghue DJ. KIDs rule: regulatory phosphorylation of RTKs. Trends in Biochemical Sciences. 2013: 38; 75–84.
9. Taylor SS, Kornev AP. Protein kinases: evolution of dynamic regulatory proteins. Trends in Biochemical Sciences. 2011: 36; 65–77.
10. Matsumoto T, Bohman S, Dixelius J, Berge T, Dimberg A, Magnusson P, Wang L, Wikner C, Qi JH, Wernstedt C, Wu J, Bruheim S, Mugishima H, Mukhopadhyay D, Spurkland A and Claesson-Welsh L. VEGF receptor-2 Y951 signaling and a role for the adapter molecule TSAd in tumor angiogenesis. The EMBO Journal. 2005: 24; 2342-2353.
11. Kendall RL, Rutledge RZ, Mao X, Tebben AJ, Hungate RW and Thomas KA. Vascular Endothelial Growth Factor Receptor KDR Tyrosine Kinase Activity Is Increased by Autophosphorylation of Two Activation Loop Tyrosine Residues. Journal of Biological Chemistry. 1999: 274; 6453–6460.
12. Waltenberger J, Claesson-Welsh L, Siegbahn A, Shibuya M and Heldin CH. Different signal transduction properties of KDR and Flt1, two receptors for vascular endothelial growth factor. Journal of Biological Chemistry. 1994: 269; 26988–26995.
13. Roskoski R. Structure and regulation of Kit protein-tyrosine kinase—The stem cell factor receptor. Biochemical and Biophysical Research Communications. 2005: 338; 1307–1315.
14. Chow LQM, Eckhardt SG. Sunitinib: From Rational Design to Clinical Efficacy. Journal of Clinical Oncology. 2007: 25; 884–896.

15. Udhaya LB, Sangeetha N, Manisha P, Ramkumar K, Kavitha M and Sabina EP. Virtual Screening of Peptidyl Arginine Deiminase Type 4 Inhibiting Potential of Chosen Flavonoids. Research Journal of Pharmacy and Technology. 2018: 11; 753–757.
16. Suganya J, Manoharan S, Radha M, Singh N and Francis A. Identification and Analysis of Natural Compounds as Fungal Inhibitors from Ocimum sanctum using in silico Virtual Screening and Molecular Docking. Research Journal of Pharmacy and Technology. 2017: 10; 3369–3374.
17. Suganya J, Radha M, Manoharan S, Vinoba V and Francis A. Virtual Screening and Analysis of Bioactive Compounds of Momordica charantia against Diabetes using Computational Approaches. Research Journal of Pharmacy and Technology. 2017:10; 3353–3360.
18. Madhumathi G, Anbarasu K and Jayanthi S. Computational Insights on Inhibition of MSH3 Induced DNA Repair with Reserpine Analogs. Research Journal of Pharmacy and Technology. 2018: 11; 3765-3768.
19. Barua A, Kesavan K and Jayanthi S. Molecular Docking Studies of Plant Compounds to Identify Efficient Inhibitors for Ovarian Cancer. Research Journal of Pharmacy and Technology. 2018: 11; 3811-3815.
20. Kumar KA, Jagannath P and Saleshier MF. Discovery of Novel Flavonoid Analogues as Angiotensin Converting Enzyme Inhibitors based on Pharmacophore Modelling and Virtual Screening Techniques. Research Journal of Pharmacy and Technology. 2018: 11; 4370-4378.
21. Anbarasu K, Senthilkumar D and Jayanthi S. Deciphering the impact of R324L Mutation in Polycystin-1PKD Domain associated with Autosomal Dominant Polycystic Kidney Disease (ADPKD): A Molecular Dynamics Perspective. Research Journal of Pharmacy and Technology. 2017: 10; 3089–3094.
22. Kesavan K, Jayanthi S. Structure Based Virtual Screening and Molecular Dynamics Studies to Identify Novel APE1 Inhibitor from Seaweeds as Anti-glioma Agent. Research Journal of Pharmacy and Technology. 2017: 10; 2474–2478.
23. Singh K, Rambabu M and Jayanthi S. Designing BRAF specific inhibitors against melanoma. Research Journal of Pharmacy and Technology. 2018: 11; 3494-3498.
24. Shankari B, Rambabu M and Jayanthi S. Identification and Designing Inhibitors for Hepatocellular Carcinoma by Targeting Claudin-10. Research Journal of Pharmacy and Technology. 2018: 11; 3529-3533.
25. Wolber G, Langer T. LigandScout: 3-D Pharmacophores Derived from Protein-Bound Ligands and Their Use as Virtual Screening Filters. Journal of Chemical Information and Modeling. 2005: 45; 160–169.
26. Hodous BL, Geuns-Meyer SD, Hughes PE, Albrecht BK, Bellon S, Bready J, Caenepeel S, Cee VJ, Chaffee SC, Coxon A, Emery M, Fretland J, Gallant P, Gu Y, Hoffman D, Johnson RE, Kendall R, Kim JL, Long AM, Morrison M, Olivieri PR, Patel VF, Polverino A, Rose P, Tempest P, Wang L, Whittington DA and Zhao H. Evolution of a Highly Selective and Potent 2-(Pyridin-2-yl)-1,3,5-triazine Tie-2 Kinase Inhibitor. Journal of Medicinal Chemistry. 2007:50; 611–626.
27. Mysinger MM, Carchia M, Irwin JJ and Shoichet BK. Directory of Useful Decoys, Enhanced (DUD-E): Better Ligands and Decoys for Better Benchmarking. Journal of Medicinal Chemistry. 2012: 55; 6582–6594.
28. Irwin JJ, Sterling T, Mysinger MM, Bolstad ES and Coleman RG. ZINC: A Free Tool to Discover Chemistry for Biology. Journal of Chemical Information and Modeling. 2012: 52; 1757–1768.
29. Sunseri J, Koes DR. Pharmit: interactive exploration of chemical space. Nucleic Acids Research. 2016: 44; W442–W448.
30. Li H, Leung K and Wong M. idock: A multithreaded virtual screening tool for flexible ligand docking. in 2012 IEEE Symposium on Computational Intelligence in Bioinformatics and Computational Biology (CIBCB). 2012: 77–84.
31. Sensharma P, Anbarasu K and Jayanthi S. In silico Identification of Novel Inhibitors against Plasmodium falciparum Triosephosphate Isomerase from Anti-Folate Agents. Research Journal of Pharmacy and Technology. 2018: 11; 3367-3370.
32. Arba M, Nur-Hidayat A, Surantaadmaja SI and Tjahjono DH. Pharmacophore-based virtual screening for identifying β5 subunit inhibitor of 20S proteasome. Computational Biology and Chemistry. 2018: 77; 64–71.
33. Case DA, Cheatham III TE, Darden T, Gohlke H, Luo R, Merz Jr. KM, Onufriev A, Simmerling C, Wang B and Woods RJ. The Amber biomolecular simulation programs. Journal of Computational Chemistry. 2005: 26; 1668–1688.
34. Salomon-Ferrer R, Götz AW, Poole D, Le Grand S and Walker RC. Routine microsecond molecular dynamics simulations with AMBER on GPUs. 2. Explicit solvent particle mesh ewald. Journal of Chemical Theory and Computation. 2013: 9; 3878–3888.
35. Maier JA, Martinez C, Kasavajhala K, Wickstrom L, Hauser KE and Simmerling C. ff14SB: Improving the Accuracy of Protein Side Chain and Backbone Parameters from ff99SB. Journal of Chemical Theory and Computation. 2015: 11(8); 3696-3713.
36. Wang JM, Wolf RM, Caldwell JW, Kollman PA and Case DA. Development and testing of a general amber force field. Journal of Computational Chemistry. 2004: 25; 1157–1174.
37. Jakalian A, Jack DB and Bayly CI. Fast, efficient generation of high-quality atomic charges. AM1-BCC model: II. Parameterization and validation. Journal of Computational Chemistry. 2002: 23; 1623–1641.
38. Arba M, Ihsan S and Tjahjono DH. Computational approach toward targeting the interaction of porphyrin derivatives with Bcl-2. Journal of Applied Pharmaceutical Science. 2018: 8; 60–66.
39. Arba M, Ruslin, Kalsum WU, Alroem A, Muzakkar MZ, Usman I and Tjahjono DH. QSAR, Molecular Docking and Dynamics Studies of Quinazoline Derivatives as Inhibitor of Phosphatidylinositol 3-Kinase. Journal of Applied Pharmaceutical Science. 2018: 8(5); 001–009.
40. Morris GM, Goodsell DS, Halliday RS, Huey R, Hart WE, Belew RK and Olson AJ. Automated docking using a Lamarckian genetic algorithm and an empirical binding free energy function. Journal of Computational Chemistry. 1998: 19; 1639–1662.